POLYOXOMETALATES

Open Access
RESEARCH ARTICLE

# Construction of PMoV/rGO/Pt nanocomposite with photoreduced graphene oxide for efficient quantification of vanillic acid

Shixu Chen, Na Li, Cong Zhang✉, Haiyan Zhao✉, Min Cui, and Bao Sun

*Hebei Provincial Key Laboratory of Photoelectric Control on Surface and Interface, School of Sciences, Hebei University of Science and Technology, Shijiazhuang 050018, China*

Cite This: *Polyoxometalates*, **2025**, *4*, 9140088

Read Online

**ABSTRACT:** Polyoxometalates (POMs), as a unique type of metal–oxygen cluster compound, undergo multi-electron transfer while maintaining their structures. In this study, an electrochemical sensor that rapidly and sensitively detects vanillic acid was synthesized using vanadium-substituted POM ($H_4PMo_{11}VO_{40}$, PMoV), reduced graphene oxide (rGO), and platinum (Pt) nanoparticles, where PMoV acted as both the photoreductant and stabilizer. In particular, PMoV/rGO/Pt composite was prepared and identified using various methods. Under optimal conditions, the limit of detection of the synthesized electrochemical sensor was estimated to be 0.9 μM at vanillic acid concentrations of 50–1350 μM. In addition, the practical application of PMoV/rGO/Pt/GCE (GCE = glassy carbon electrode) was considered by determining the concentration of vanillic acid in tap and lake water with good recovery (98.36%–102.11% and 97.11%–100.22%, respectively). The synthesized sensor realizes simple, rapid, and economical detection of vanillic acid and can serve as an important analytical tool in this direction.

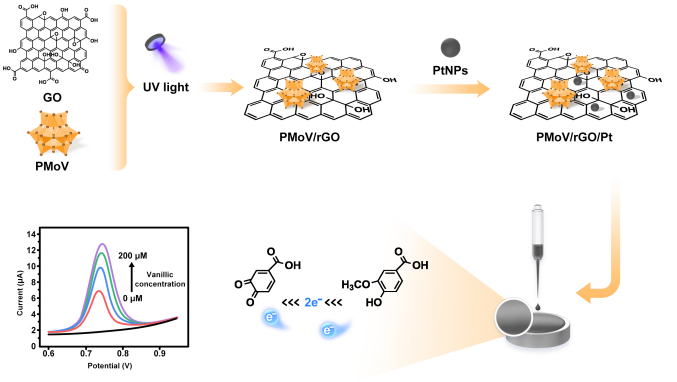


**KEYWORDS:** polyoxometalates, vanillic acid, electrochemistry, sensor, photoreductant

## 1 Introduction

Vanillic acid (VA = 4-hydroxy-3-methoxybenzoic acid) is a compound with a phenolic acid structure and is commonly derived from the secondary metabolism of fruits, plants, and vegetables [1–3]. Phenolic compounds contain scavenging free radicals and exhibit anticancer, diabetes resistance, antioxidant, antibacterial, and anti-inflammatory properties. Therefore, phenolic acid compounds are thought to provide various health benefits [4, 5]. According to research, the presence of phenolic compounds in fruits, vegetables, and other plant products significantly contributes to their protective characteristics [6, 7]. VA is extensively used in the composition of various food and pharmaceutical products [8, 9]. For example, VA is an antibacterial component of Radix coptis, and the amount of VA in it can be used as an index to measure the quality of Radix coptis. Therefore, it is necessary to develop simple, fast, and sensitive analytical methods for efficiently and quantitatively detecting phenolic compounds in complex substrates. Current VA detection methods include liquid chromatography, capillary electrophoresis, spectroscopy, and electrochemical sensing. Compared with other detection methods, electrochemical sensing has the advantages of simple operation, low cost, and high sensitivity [10–14]. In addition, another advantage of the electrochemical detection method is that different materials can be used to modify the electrode to improve analytical detection performance.

Because of its large specific surface area and superior mechanical properties, reduced graphene (rGO) provides numerous active sites and exhibits enhanced material properties, which broadens its application prospects in energy storage, composite materials, and biomedicine [15, 16]. Therefore, the oxidation and subsequent reduction of graphene to rGO can improve its performance and expand its application range. Until now, research on graphene reduction methods has primarily focused on chemical reduction, thermal annealing, and photoreduction [17–21]. However, conventional chemical reduction and thermal annealing methods suffer from environmental pollution and operational difficulty [22].

Polyoxometalates (POMs) are a class of transition metal–oxygen clusters with rich structural versatility and excellent redox properties. They have been extensively used in catalysis, medicine, biology, and other research fields [23–26]. More importantly, the removal of one, two, or more complement metal atoms from

**Received:** July 26, 2024; **Revised:** March 12, 2025
**Accepted:** March 22, 2025

✉Address correspondence to Cong Zhang, zhangcong0672@163.com; Haiyan Zhao, yanzi977649230@163.com

https://doi.org/10.26599/POM.2025.9140088

POMs can be controlled by adjusting the pH or ionic strength of the solution and introducing other metal atoms to form substituted POMs [27, 28]. Vanadium is a common impurity atom. The introduction of vanadium atoms into the classical acid structure can increase the surface charge density of the anions of POM clusters and enrich the electrochemical properties of the salts [29–31]. This result is attributed to the oxidation order of the complement atoms in the Keggin structure: $V^{V}$ > $Mo^{VI}$ > $W^{VI}$ [32–34]. Therefore, replacing Mo atoms in phosphomolybdic acid with vanadium atoms improves the oxygen reduction activity of the catalyst. Recently, researchers have achieved the photoreduction of graphene by irradiating graphene with ultraviolet (UV) light. This method is not only environmentally friendly but also easy to control [35, 36]. Under UV irradiation, graphene oxide (GO) undergoes photocatalytic reduction with POMs to form a composite of rGO and POMs [37].

In this study, we prepared vanadium-substituted phosphomolybdic acid as a catalyst for the photoexcitation of vanadium-substituted POMs ($H_4PMo_{11}VO_{40}$, PMoV) under UV irradiation to produce heteropoly blue. Heteropoly blue can then transfer electrons to the graphene redox, which is reduced to rGO, eventually producing a composite material containing rGO and PMoV. Thus, the specific surface area of the composite is increased, and more active sites are loaded. In the composite material, we introduced platinum (Pt) nanoparticles (NPs) as a suitable catalyst to reduce the overpotential of VA oxidation and enhance electrical conductivity and sensitivity.

## 2 Experimental

### 2.1 Materials

Sodium metavanadate ($NaVO_3$), sodium molybdate dehydrate ($Na_2MoO_4{\cdot}H_2O$), sodium phosphate tribasic dodecahydrate ($Na_3PO_4{\cdot}12H_2O$), and sodium borohydride ($NaBH_4$) were obtained from Aladdin Chemistry Co., Ltd. (Shanghai, China). Potassium hexachloroplatinate ($K_2PtCl_6$) was obtained from Sigma-Aldrich Co. $Na_2HPO_4$ and $NaH_2PO_4$ were purchased from Tianjin Damao Chemical Reagent Co. (China). All reagents were of analytical grade and were used as received. All aqueous solutions were prepared using doubly distilled water.

### 2.2 Methods

The obtained nanocomposites were characterized by transmission electron microscopy (TEM, JEM-2100, Japan), X-ray diffraction (XRD, Rigaku, D/max-rA, Japan), Fourier transform infrared (FT-IR) spectroscopy (TENSOR 37, Bruker, Germany), and X-ray photoelectron spectroscopy (XPS, Escalab 250Xi, USA).

Electrochemical experiments were conducted using an electrochemical workstation (CHI660D, Shanghai, China) with a conventional three-electrode system with the modified electrode as the working electrode, a Pt wire (1 mm diameter) as the counter electrode, and an Ag/AgCl electrode (saturated with KCl) as the reference electrode.

### 2.3 Synthesis of PMoV

PMoV was prepared using a previously reported method [38]. $NaVO_3$ (0.01 mol, 1.22 g) was dissolved in 20-mL $H_2O$. $Na_3PO_4{\cdot}12H_2O$ (0.01 mol, 3.8 g) was dissolved in 50-mL $H_2O$ and slowly added to the above solution to obtain a mixed solution. The solution pH was adjusted to 5 with 1:1 dilute $H_2SO_4$, and the solution was then heated at 90 °C for 30 min. $Na_2MoO_4{\cdot}2H_2O$ (0.1 mol, 24.2 g) was added to the reaction solution, and the pH was adjusted to 2.5. The mixed solution was heated for 180 min and then cooled to room temperature. The solution was extracted with 50-mL ether and an appropriate amount of $H_2SO_4$ (1:1). The obtained red oily heteropolyether compound was located in the middle layer. This process was repeated until the water phase became pale yellow. The red oil was dissolved in 50 mL of distilled water. Finally, the formed large red crystals were filtered, washed, and air-dried to obtain PMoV.

### 2.4 Synthesis of GO

GO was prepared from natural graphite powder via acid oxidation using a modified Hummers' method [39]. First, 23 mL of $H_2SO_4$ was placed in a conical bottle, and 0.5 g of sodium nitrate and 1 g of natural graphite powder were slowly added to the conical bottle with stirring until the mixture was well combined. Three portions of 1-g potassium permanganate were poured into a conical bottle. The solution gradually turned dark green. The solution was stirred in an ice bath for 120 min. Subsequently, the solution was heated and stirred in a water bath for 120 min. Then, 50 mL of steamed water was added to the reaction system, and the temperature was raised to 98 °C for 20 min. The solution was brown with purplish-red smoke. Finally, 5-mL hydrogen peroxide was added to stop the oxidation reaction, and the reaction was stopped after continuous stirring for 30 min, at which time the solution became bright yellow. The distilled water was centrifuged several times until the pH was neutral and the filtrate was free of sulfate. Dark brown GO was obtained by drying at 80 °C (referred to as GO).

### 2.5 Synthesis of PMoV/rGO

For the preparation of PMoV/rGO nanocomposites, PMoV was first photochemically reduced using a UV lamp. PMoV (4 mg·mL$^{-1}$) was mixed with isopropanol (300 μL), and GO (500 μL, 2 mg·mL$^{-1}$) was then added to the mixed solution. The resulting solution was stirred, and Ar was used to remove oxygen for 30 min. The mixture was then exposed to UV light for 80 min. The UV-irradiated solution was transferred to a centrifuge tube for later use (marked as PMoV/rGO).

### 2.6 Synthesis of PMoV/rGO/Pt

20 mg of $K_2PtCl_6$ was dissolved in 10-mL deionized (DI) water with stirring for 1 h. The freshly prepared aqueous $NaBH_4$ solution was added dropwise and stirred for 2 h. The NPs were obtained by centrifugation, washing, and drying at 60 °C [40]. The dispersing solution PMoV/rGO was mixed uniformly by adding an equal volume of DI water. Pt NPs (1 mg·mL$^{-1}$) were added to the mixed solution for ultrasonication. An ultrasonic homogeneous mixture (denoted PMoV/rGO/Pt) was used to modify the electrode.

### 2.7 Preparation of modified electrodes

First, the glassy carbon electrode (GCE) was successively polished with 0.3- and 0.05-μm α-alumina powder and subsequently cleaned in water and ethanol via multiple ultraphonic operations until the potential difference was less than 90 mV. The PMoV/GO, PMoV/rGO, and PMoV/rGO/Pt aqueous solutions were then prepared and treated via ultrasonication until homogeneous solutions were formed. Subsequently, a 6-μL solution was applied to the surface of the GCE electrode by drop-casting, and the surface

was dried at room temperature. The formed electrodes were recorded as PMoV/GO/GCE, PMoV/rGO/GCE, and PMoV/rGO/Pt/GCE. Scheme 1 shows the synthesis process of a VA sensor.

## 3 Results and discussion

### 3.1 Characterization of composites

The structures and morphologies of the modified materials were investigated using TEM, EDS, XPS, XRD, and FT-IR analyses.

Figure 1(a) shows the TEM image of the PMoV/rGO/Pt composite. PMoV has an irregular shape. The rGO sheets exhibit a thin lamellar structure and are covered by PMoV and PtNPs. The black-spotted Pt NPs are distributed on the rGO surface. As shown in the high-resolution TEM (HRTEM) image (Fig. 1(b)), the spacing of the adjacent lattice fringes is 0.22 nm, which corresponds to the (111) crystal plane of the Pt NPs, and most of the synthesized Pt NPs exhibit a spacing of 4 nm. POM clusters can be adsorbed on rGO [41]. The electrostatic repulsion between negatively charged POMs prevents Pt NPs from aggregating. We conducted energy spectrum scanning (EDS mapping) of the PMoV/rGO/Pt sample (Fig. S1 in the Electronic Supplementary Material (ESM)). As shown in the diagram, elements P, Mo, V, and Pt are present throughout the selected sample.

To further verify the chemical composition of the PMoV/rGO/Pt composite, XPS analysis was performed. The characteristic peaks in the XPS survey spectrum for PMoV/rGO/Pt corresponded to the elements of C, Mo, P, V, and Pt in the nanocomposites, as shown in Figs. 2(a)–2(f). The C 1s peaks were observed with binding energies of 284.8 eV (C–C/C=C from rGO) and 288.0 eV (a small amount of O–C=O in rGO) (Fig. 2(b)). The Mo 3d core level spectrum features two signals at binding energies of 231.4 and 234.5 eV, corresponding to the Mo $3d_{3/2}$ and Mo $3d_{5/2}$ of PMoV, respectively, indicating Mo with a valence state of +6 [42, 43]. The binding energy peak of V 2p is 517 eV, proving the existence of V and indicating the successful synthesis of PMoV. The Pt 4f signals of PMoV/rGO/Pt exhibit two binding energy peaks at 71.0 and 75.1 eV. Based on the SEM, TEM, and XPS results, the PMoV/rGO/Pt composite nanomaterials were successfully prepared.

The crystalline structures of PMoV, PMoV/rGO, and PMoV/rGO/Pt were characterized by powder XRD. As shown in Fig. 3, after the photoreduction process, the diffraction peak of GO (10.87°) disappeared [44]. However, the peak of newly generated rGO overlaps that of POMs, which makes the peak of rGO unrecognizable. In addition, the XRD pattern of PMoV/rGO/Pt exhibited additional distinguishable peaks at 39.71° and 46.22°, which agree well with the reflections from the (111) and (200) planes of Pt (PDF#04-0802) [40]. The XRD and TEM results showed that the Pt NPs were successfully attached to the PMoV/rGO/Pt composite without damaging the PMoV/rGO structure. The IR (Fig. S2 in the ESM) shows that PMoV exhibits four characteristic peaks within the range of 800–1100 $cm^{-1}$, namely, 1060 $cm^{-1}$ (P–O), 961 $cm^{-1}$ (Mo–$O_t$), 865 $cm^{-1}$ (Mo–$O_c$–Mo), and 776 $cm^{-1}$ (Mo–$O_e$–Mo), 1568 $cm^{-1}$ (C=C, C–N), and 3382 $cm^{-1}$ (O–H). The four characteristic peaks still exist after recombination, demonstrating that the crystal structure stability of POMs is maintained after reduction to heteropoly blue.

### 3.2 Electrochemical behavior of modified electrodes

The electrochemical behavior of bare GCE, PMoV/GO/GCE, PMoV/rGO/GCE, and PMoV/rGO/Pt/GCE in a mixed solution of 5-mM $[Fe(CN)_6]^{3-}$ and 0.1 M KCl was investigated by cyclic voltammetry (CV). The results are presented in Fig. 4. The four electrodes exhibited a pair of redox peaks, and their peak currents were ranked as follows: PMoV/rGO/Pt/GCE > bare GCE > PMoV/rGO/GCE > PMoV/GO/GCE. The low current of PMoV/GO/GCE is attributed to the poor conductivity of GO with more carboxyl and hydroxyl groups. With the reduction of GO by POM photoreduction, the surface functional groups of GO are reduced, the electrical conductivity of PMoV/rGO/GCE is improved, and the current is increased. POMs successfully reduced GO to rGO using a simple photoreduction method. The current of the modified PMoV/rGO/Pt/GCE electrode was significantly increased compared to that of the GCE because the introduction of Pt NPs increased the conductivity of the modified electrode. Therefore, the peak current of PMoV/rGO/Pt/GCE was higher than that of the bare GCE.

Electrochemical impedance spectroscopy (EIS) was used to further observe the conductivity of the electrodes. EIS experiments were conducted using a solution containing 5-mM $[Fe(CN)_6]^{3-/4-}$ and 0.1-M KCl. The EIS data of the modified electrodes were simulated using electrical equivalent circuit models using the ZSimpWin software. The results are presented in Fig. 4(b). Based on the calculation results, the charge transfer resistance ($R_{ct}$) values

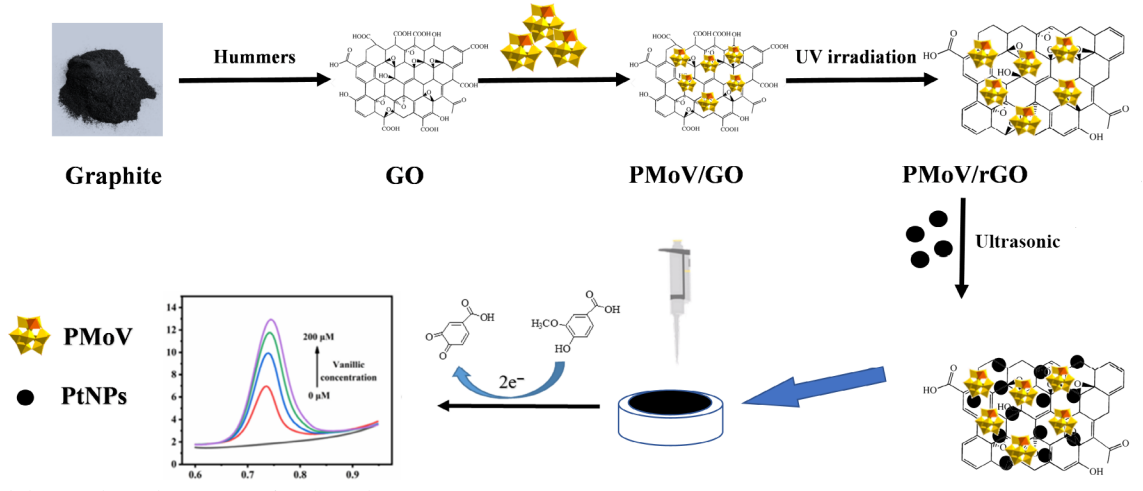


**Scheme 1** Shcheme 1 The synthesis process of vanillic acid sensor.

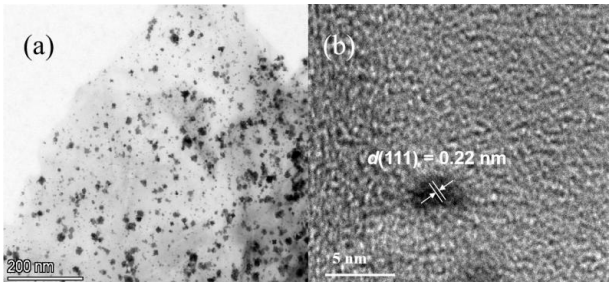


**Figure 1** (a) TEM and (b) HTREM images of PMoV/rGO/Pt.

of PMoV/rGO/Pt/GCE, bare GCE, PMoV/rGO/GCE, and PMoV/GO/GCE are 41.16, 130.6, 333.2, and 374.2 Ω, respectively. The trend of the Rct values of different modified electrodes can be compared with the CV trend in a typical $[Fe(CN)_6]^{3-}$ solution. Because of the numerous functional groups on the GO surface, the resistance value of the PMoV/GO-modified electrode was the highest. With the introduction of photoreduction and Pt NPs, the resistance value of the modified electrode gradually decreased. In conclusion, the modified electrode based on the final composite PMoV/rGO/Pt exhibits excellent electrochemical properties and can be used to fabricate highly efficient and sensitive sensors.

Due to the excellent electrical conductivity of PMoV/rGO/Pt/GCE, we evaluated whether an electrochemical sensor can be used for VA detection. The CV results of the modified electrodes in a Britton-Robinson (B-R) buffer solution containing 0.1-mM VA at a scanning rate of 100 $mV \cdot s^{-1}$ are presented in Fig. 5(a). When VA was added, bare GCE detected a low oxidation peak current, whereas PMoV/GO/GCE detected a higher oxidation peak current of VA. Compared with PMoV/GO/GCE, PMoV/rGO/GCE exhibited a higher oxidation peak current because its conductivity was improved. After the addition of Pt NPs, the overpotential of the reaction was reduced, making VA more easily oxidized, and the peak potential shifted to the left. The oxidation peak current of VA was significantly improved. Therefore, PMoV/rGO/Pt/GCE effectively detects VA and exhibits the highest response current among all electrodes. In addition, differential pulse voltammetry (DPV) was used to test the B-R buffer solution without VA by PMoV/rGO/Pt/GCE, and no oxidation peak current of VA was observed. When a certain amount of VA was added continuously, the oxidation peak current gradually increased, indicating VA.

### 3.3 Optimization of experimental conditions

The experiment was conducted by optimizing the content and reduction time of GO, the ratio between the composites, the amount of electrode drop coating, and the pH of the buffer solution to obtain the highest vanillate current.

The experiment explored the addition of different volumes of GO. Specifically, 100, 300, 500, 700, and 900 μL of GO (2 $mg \cdot mL^{-1}$) were added to the PMoV dispersion. GO was photoreduced by UV irradiation, and the VA was electrochemically tested using PMoV/rGO/Pt/GCE (Fig. S3(a) in the ESM). The current was highest when 500 μL of GO was added. Then, the illumination time was also optimized. The results are presented in Fig. S3(b) in the ESM. As the illumination time increased, the measured current gradually increased and then flattened out after reaching a certain height. This result was due to the gradual reduction of GO to rGO by PMoV after light exposure. After a certain time, the GO in the solution was converted to rGO; thus, the current did not increase and tended to be flat. Therefore, we added 500 μL of GO and irradiated it with UV light for 80 min. The subsequent materials were processed under these optimal conditions.

The amount of Pt NPs introduced also affects the electrochemical response of VA. In this experiment, dispersions of the same concentration were mixed to modify the electrodes in different volumes. To determine the optimal ratio of PMoV/rGO to Pt NPs, the volume of PMoV/rGO was fixed in this experiment, and different volumes of Pt NPs were added. The current responses of the composites with different volume ratios to VA were tested (Fig. S4(a) in the ESM). The current was highest at $V_{PMoV/rGO}$:$V_{Pt}$ =

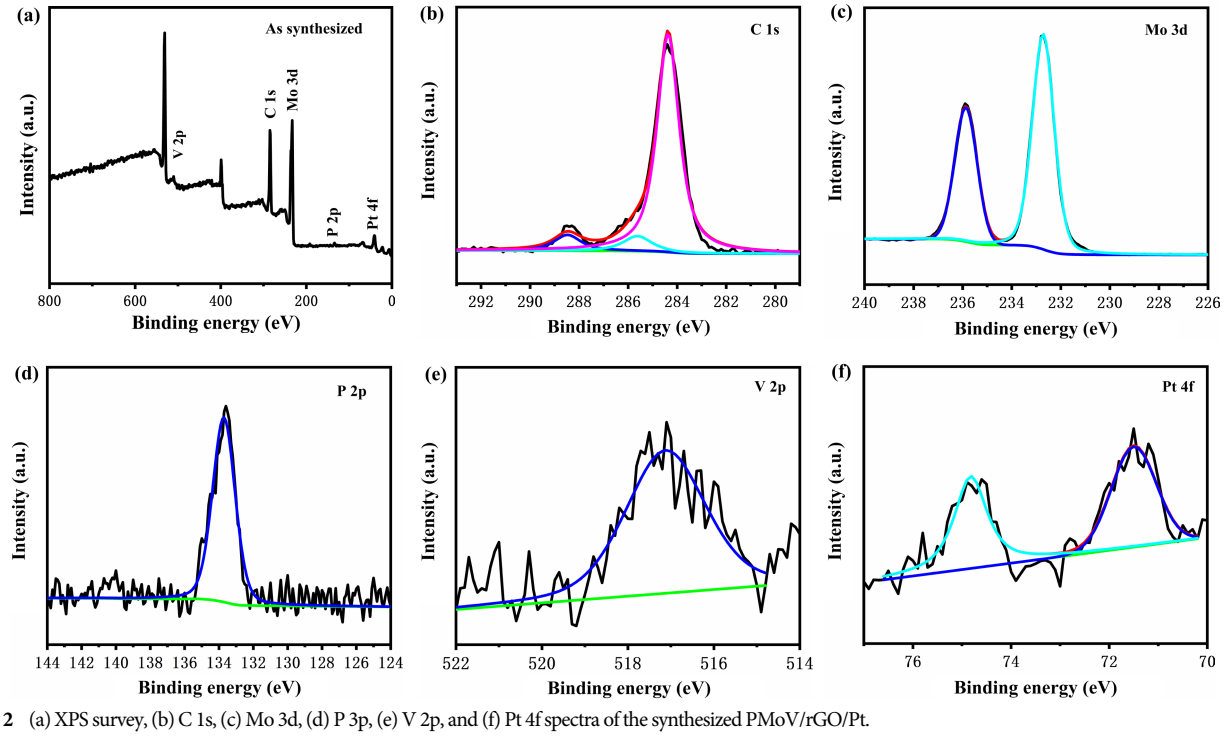


**Figure 2** (a) XPS survey, (b) C 1s, (c) Mo 3d, (d) P 3p, (e) V 2p, and (f) Pt 4f spectra of the synthesized PMoV/rGO/Pt.

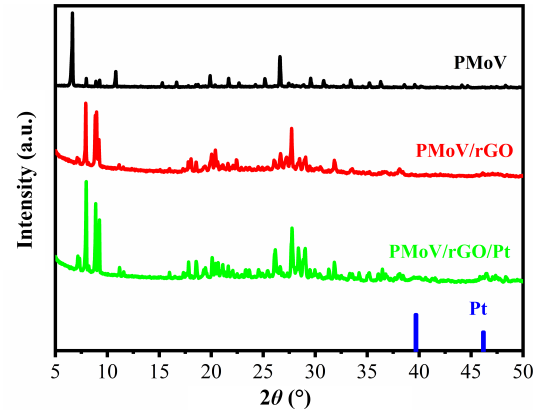


**Figure 3** Powder XRD patterns of PMoV, PMoV/rGO, PMoV/rGO/Pt and JCPDS of Pt.

7:1. The introduction of Pt NPs gradually improved the conductivity of the material; however, after a certain concentration, additional Pt NPs caused agglomeration and affected the current response. After determining the optimum volume mixing ratio, the drop-coating weight of PMoV/rGO/Pt was optimized because the modification material on the electrode being either too thin or thick affected the electron transfer rate. By adding a certain gradient of PMoV/rGO/Pt, the optimal amount of drop coating was 8 μL (Fig. S4(b) in the ESM).

To further explore the effect of different pH values of the buffer solution on the experimental results, the electrochemical behavior of VA at the modified electrode interface was explored using the CV method in a B-R buffer solution with different pH values. This experiment explored the influence of pH between 2 and 4 on the experimental results. The peak current was highest at pH 2.5, furthermore, as the pH increased, the peak potential gradually shifted to left (Figs. S5(a) and S5(b) in the ESM), indicating that protons participated in the electrocatalytic process. A good linear relationship is observed between the peak potential $E_p$ and pH (Fig. S5(c) in the ESM), and the linear equation is given by $E_p = -0.0516\text{pH} + 0.947$ ($R^2 = 0.997$), which has excellent linearity. According to the Nernst equation, the relationship between $E_p$ and pH is expressed as follows:

$$E_p = \frac{0.059m}{n}\text{pH} + b \quad (1)$$

The slope between $E_p$ and pH is 0.0516, implying that each pH 0.0516 V slope is close to the theoretical value of each pH 0.059 V. This means that the value of $m$ is approximately equal to that of $n$. This result suggests that the electrochemical reaction of VA involves an equal number of protons and electrons.

The effect of scan rate on PMoV/rGO/Pt/GCE was investigated by CV in a B-R buffer solution containing 0.1-mM VA. The experimental results demonstrated that the oxidation peak current of VA increased as the scan rate increased from 10 to 200 mV·s$^{-1}$, and the peak potential shifted to a positive potential (Fig. 6(a)). The oxidation peak currents of VA were linearly related to the square root of the scan rate, indicating that the reaction process is diffusion-controlled (Fig. 6(b)). Considering experimental stability and

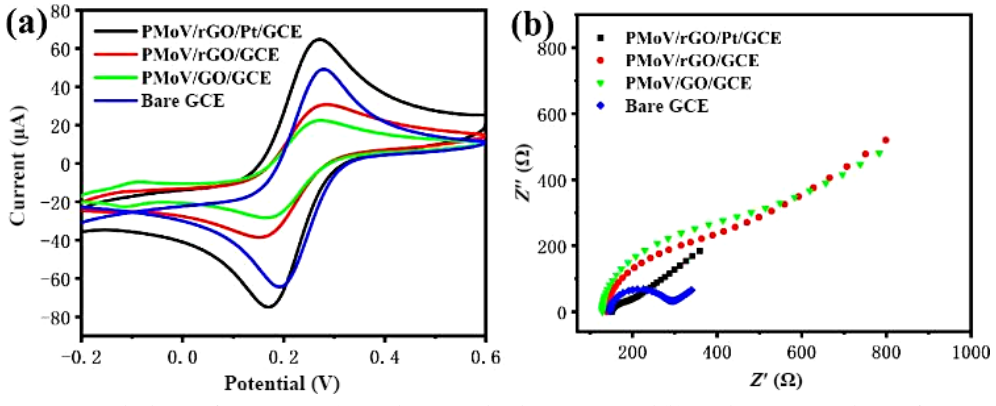


**Figure 4** (a) CV diagram in a mixed solution of 5 mM $[Fe(CN)_6]^{3-}$ and 0.1 M KCl with 100 mV·s$^{-1}$ and (b) EIS diagrams in a solution of 5 mM $[Fe(CN)_6]^{3-/4-}$ and 0.1 M KCl of different modified electrodes.

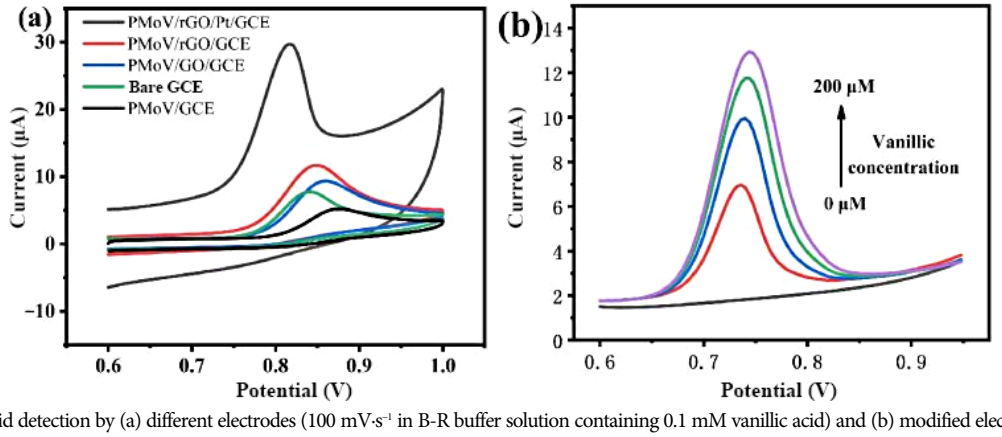


**Figure 5** Vanillic acid detection by (a) different electrodes (100 mV·s$^{-1}$ in B-R buffer solution containing 0.1 mM vanillic acid) and (b) modified electrodes (100 mV·s$^{-1}$ in B-R buffer solution containing different concentrations vanillic acid).

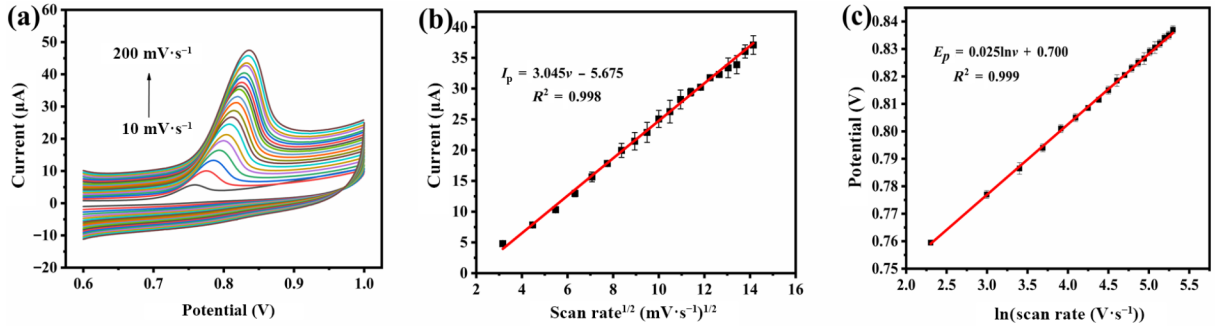


**Figure 6** (a) The influence of different sweep speed on peak current (B-R buffer solution containing 0.1 mM vanillic acid). (b) The linear relationship of current and the square root of sweep speed. (c) The relationship between ln(scan rate) and peak current.

sensitivity, 100 mV·s$^{-1}$ was selected for subsequent experiments. In addition, as shown in Fig. 6(c), $E_p$ increased as the logarithm of the scanning speed increased and exhibited a good linear relationship ($R^2$ = 0.999) at scanning speeds of 10–200 mV·s$^{-1}$. For irreversible oxidation reactions, $E_p$ can be expressed by the following Laviron equation:

$$E_p = E^\theta + (RT/\alpha nF)\ln(RTk^\theta/\alpha nF) + (RT/\alpha nF)\ln v \quad (2)$$

Here, $n$ represents the number of electrons involved in the charge transfer step, $\alpha$ denotes the transfer coefficient ($\alpha$ is assumed to be 0.5 in a completely irreversible electrode process), $v$ represents the potential scanning rate, and $E^\theta$ denotes the formal potential. Other symbols have their usual meanings. $R$ is molar gas constant, $T$ is thermodynamic temperature, $F$ is faraday constant, $k^\theta$ standard rate constant. Therefore, the value of $\alpha n$ can be easily calculated from the slope of $E_p$–ln$v$. In this system, the slope was 0.025; thus, the value of $\alpha n$ was calculated as 1.027. Therefore, the number of electrons transferred ($n$) was approximately 2. From the relationship between $E_p$ and pH, we know that the numbers of protons and electrons transferred during the reaction were the same. The reaction mechanism of VA on PMoV/rGO/Pt/GCE can be proved using Eqs. (3)–(5) [45, 46]

$$[PMo_{11}^{VI}V^{V}O_{40}]^{4-} + e^- \rightarrow [PMo_{11}^{VI}V^{IV}O_{40}]^{5-} \quad (3)$$

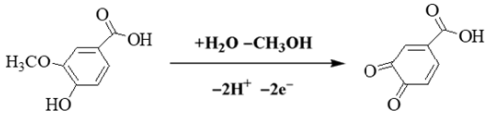


(4)

In summary, the electrocatalytic oxidation reaction of VA at PMoV/rGO/Pt/GCE was assumed to proceed as follows:

$$2[PMo_{11}VO_{40}]^{4-} + C_8H_8O_4 + H_2O \rightarrow 2[PMo_{11}VO_{40}]^{5-} + C_7H_4O_4 + CH_3OH + 2H^+ \quad (5)$$

### 3.4 Electrochemical determination of VA

DPV was used to quantitatively determine VA under optimum conditions. The anodic peak current increased gradually with increasing VA concentration from 50 to 1350 μM (Fig. 7(a)). Well-linear relationships between the current and the VA concentration in ranges of 50–200 μM ($R^2$ = 0.993) and 200–1350 μM ($R^2$ = 0.992) with the corresponding sensitivities of 0.039 and 0.012 μA·μM$^{-1}$, respectively, were observed (Fig. 7(b)), and the regression equations were $I_p$ = 0.03964$c$ + 2.428 and $I_p$ = 0.01215$c$ + 8.596, respectively. The limit of detection was calculated to be 0.9 μM (S/N = 3). Compared with other reported methods for detecting VA, our sensor has comparable or even better detection performance (Table 1).

### 3.5 Sensor performance consistency

To assess the selectivity of the prepared VA sensor, the interference from a structure similar to VA or with possible influence substances, including hydroquinone (HQ), catechol (CC), 2,5-dihydroxyterephthalic acid (DHTA), pureterephthalicacid (PTA), L-cysteine (L-Cys), citric acid(CA), KCl, $MgCl_2$, and $Cu(NO_3)_2$, was evaluated by DPV (Fig. 8(a)). There was no obvious interference on the current value of VA by PMoV/rGO/Pt/GCE, indicating that PMoV/rGO/Pt/GCE exhibits high VA selectivity.

In addition, the reproducibility of PMoV/rGO/Pt/GCE was investigated by measuring the response of five electrodes to 0.1-mM VA (Fig. 8(b)), and the relative standard deviation (RSD) was 2.01%. The repeatability of PMoV/rGO/Pt/GCE was determined by using it to detect VA five times in a day (Fig. 8(c)). The results show

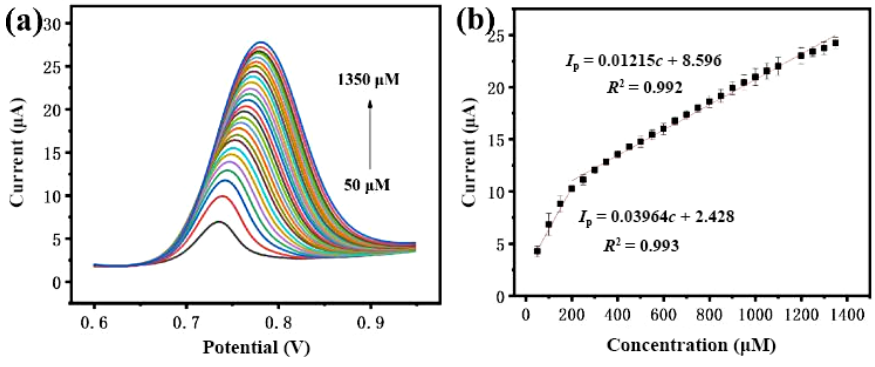


**Figure 7** (a) The effect of different concentrations on current (100 mV·s$^{-1}$ in B-R buffer solution containing 50–1350 μM vanillic acid). (b) Linear relationship between concentration and current.

**Table 1** Comparison of vanillic acid detection by different methods

| Method | Linear range | LOD | Ref. |
|---|---|---|---|
| Lc-GCE | 10–1000 μM | 7.83 μM | [47] |
| PAH-AuNPs/GCE | 0.90–15.0 μM | 0.055 μM | [48] |
| CE-DAD | 12–180 μM | 8.9 μM | [49] |
| BDD | 340–16,810 μg·mL$^{-1}$ | 30 μg·mL$^{-1}$ | [50] |
| PMoV/rGO/Pt/GCE | 50–1350 μM (8.408–227.003 μg·mL$^{-1}$) | 0.9 μM (0.151 μg·mL$^{-1}$) | This work |

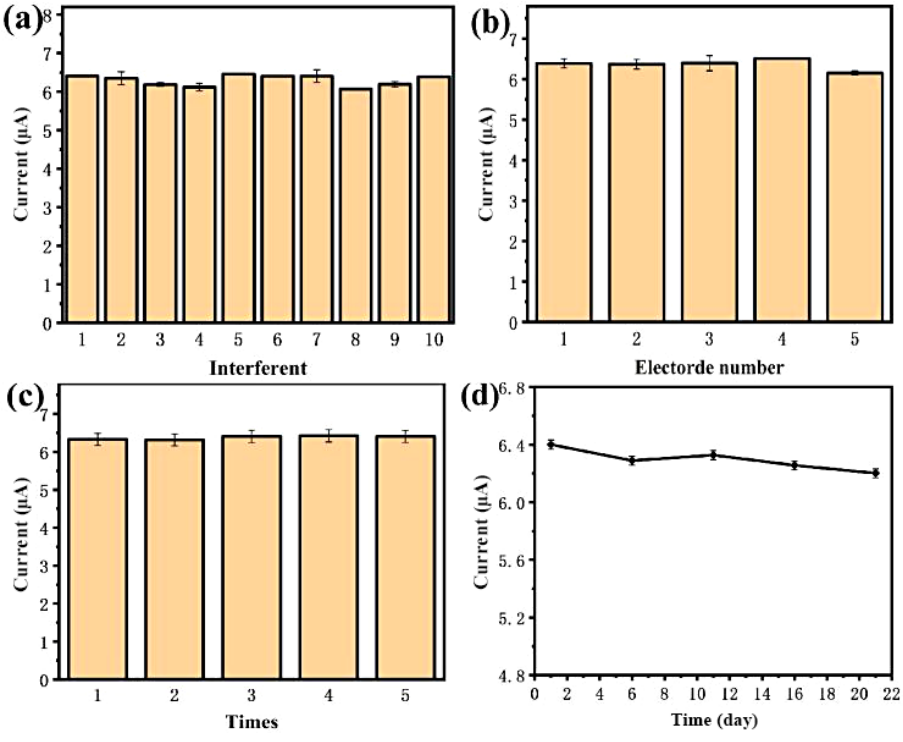


**Figure 8** The (a) selectivity (1-HQ, 2-CC, 3-DHTA, 4-PTA, 5-L-Cys, 6-CA, 7-KCl, 8-$MgCl_2$, 9-$Cu(NO_3)_2$ and 10-VA), (b) reproducibility, (c) repeatability, and (d) stability of the PMoV/rGO/Pt/GCE.

that the RSD of the PMoV/rGO/Pt/GCE is 1.18%, confirming the repeatability of the sensor for VA sensing. The stability of PMoV/rGO/Pt/GCE was evaluated every five days by measuring the current of VA (Fig. 8(d)). The current intensity remained at 95% of the initial current even after 21 days. The results show that PMoV/rGO/Pt/GCE exhibits good repeatability, reproducibility, and stability.

### 3.6 Real sample analysis

To evaluate the feasibility of the prepared sensor in practical applications, the standard addition method was used to test the sensor with real samples that may contain VA. Different VA concentrations were added to lake and tap water samples, and the response current of VA in these samples was measured by PMoV/rGO/Pt/GCE. As shown in Table 2, the recovery rates for the lake water samples ranged from 98.36% to 102.11% (RSD ranged from 1.15% to 2.12%). The recovery rates for the tap water samples ranged from 97.11% to 100.22% (RSD ranged from 2.18% to 2.56%). These results demonstrate that the PMoV/rGO/Pt/GCE sensor detects VA in real samples.

## 4 Conclusions

In this study, we successfully prepared a PMoV/rGO/Pt composite material and then a high-sensitivity electrochemical sensor for VA detection. Under UV irradiation, POMs can be transformed into heteropoly blue with a reductive state. In this state, it exhibits reducibility. Therefore, we used a simple photoreduction method to reduce GO to rGO in a POM-containing solution. After collecting PMoV/rGO, we added Pt NPs to further improve its electrical conductivity. The synergistic effect of the three compounds imparts PMoV/rGO/Pt/GCE with high sensitivity and a wide linear range. In addition, the practical detection results are satisfactory. To the best of our knowledge, the PMoV/rGO/Pt composite material has not been used to fabricate a sensor for VA detection, providing a new approach in this direction.

**Electronic Supplementary Material**: Supplementary material (EDS mapping, IR spectra, and optimization of experimental conditions) is available in the online version of this article at https://doi.org/10.26599/POM.2025.9140088.

## Data availability

All data needed to support the conclusions in the paper are presented in the manuscript and the Electronic Supplementary Material. Additional data related to this paper may be requested from the corresponding author upon request.

## Acknowledgements

The authors acknowledge the support given by the Science and Technology Project of Hebei Education Department (No. BJK2023068), the Central Guidance on Local Science and Technology Development Fund of Hebei Province (No. 226Z7715G), and the Natural Science Foundation of Hebei Province (No. B2024208050).

## Declaration of competing interest

The authors have no competing interests to declare that arerelevant to the content of this article.

## Author contribution statement

S. X. C.: Data curation, writing manuscript. N. L.: Experimental design, writing manuscript. C. Z.: Project administration, funding acquisition. H. Y. Z.: Project administration, funding acquisition. M. C.: Project administration. B. S.: Project administration. All the authors have approved the final manuscript.

## Use of AI statement

None.

## References

[1] Buffon, E.; Stradiotto, N. R. Using a disposable platform based on reduced graphene oxide, iron nanoparticles and molecularly imprinted polymer for voltammetric determination of vanillic acid in fruit peels. *Food Chem.* **2022**, *397*, 133786.

[2] Vinothiya, K.; Ashokkumar, N. Modulatory effect of vanillic acid on antioxidant status in high fat diet-induced changes in diabetic hypertensive rats. *Biomed. Pharmacother.* **2017**, *87*, 640–652.

[3] Mitić, M.; Janković, S.; Mašković, P.; Arsić, B.; Mitić, J.; Ickovski, J. Kinetic models of the extraction of vanillic acid from pumpkin seeds. *Open Chem*. **2020**, *18*, 22–30.

[4] Chuang, H. W.; Wei, I. H.; Lin, F. Y.; Li, C. T.; Chen, K. T.; Tsai, M. H.; Huang, C. C. Roles of akt and ERK in mTOR-dependent antidepressant effects of vanillic acid. *ACS Omega* **2020**, *5*, 3709–3716.

[5] Li, X. F.; Gao, Y. T.; Xiong, H. B.; Yang, Z. The electrochemical redox mechanism and antioxidant activity of polyphenolic compounds based on inlaid multi-walled carbon nanotubes-modified graphite electrode. *Open Chem.* **2021**, *19*, 961–973.

[6] Víctor-Ortega, M. D.; Fajardo, A. S.; Airado-Rodríguez, D. Sustainable development: Use of agricultural waste materials for vanillic acid recovery from wastewater. *Sustainability* **2022**, *14*, 2818.

[7] Zaripour, M.; Zare-Shahabadi, V.; Jahromi, H. J. Application of ultrasonic-assisted inclusion complex formation with α-cyclodextrin for simultaneous spectrophotometric determination of gallic acid and vanillic acids in fruit samples. *Spectrochim. Acta Part A: Mol. Biomol. Spectrosc.* **2019**, *222*, 117197.

[8] Kaur, J.; Gulati, M.; Singh, S. K.; Kuppusamy, G.; Kapoor, B.; Mishra, V.; Gupta, S.; Arshad, M. F.; Porwal, O.; Jha, N. K. et al. Discovering multifaceted role of vanillic acid beyond flavours: Nutraceutical and therapeutic potential. *Trends Food Sci. Technol.* **2022**, *122*, 187–200.

[9] Jeong, H. J.; Nam, S. Y.; Kim, H. Y.; Jin, M. H.; Kim, M. H.; Roh, S. S.; Kim, H. M. Anti-allergic inflammatory effect of vanillic acid through regulating thymic stromal lymphopoietin secretion from activated mast cells. *Nat. Prod. Res.* **2018**, *32*, 2945–2949.

[10] Xu, Z. J.; Li, P. P.; Chen, H. Y.; Zhu, X. H.; Zhang, Y. Y.; Liu, M. L.; Yao, S. Z. Picomolar glutathione detection based on the dual-signal self-calibration electrochemical sensor of ferrocene-functionalized copper metal-organic framework via solid-state electrochemistry of cuprous chloride. *J. Colloid Interface Sci.* **2022**, *628*, 798–806.

[11] Tajik, S.; Orooji, Y.; Ghazanfari, Z.; Karimi, F.; Beitollahi, H.; Varma, R. S.; Jang, H. W.; Shokouhimehr, M. Nanomaterials modified electrodes for electrochemical detection of Sudan I in food. *J. Food Measure. Charact.* **2021**, *15*, 3837–3852.

[12] Qi, Y. F.; Sun, R. M.; Lv, R. J.; Li, Y. H.; Du, T.; Chen, L. X.; Zhang, Y.; Yang, W. Polyoxometalates-graphene nanocomposites modified electrode for electro-sensing detection of sudan I in food. *Food Chem. Toxicol.* **2022**, *166*, 113222.

[13] Karimi-Maleh, H.; Darabi, R.; Shabani-Nooshabadi, M.; Baghayeri, M.; Karimi, F.; Rouhi, J.; Alizadeh, M.; Karaman, O.; Vasseghian, Y.; Karaman, C. Determination of D&C red 33 and patent blue V Azo dyes using an impressive electrochemical sensor based on carbon paste electrode modified with ZIF-8/g-$C_3N_4$/Co and ionic liquid in mouthwash and toothpaste as real samples. *Food Chem. Toxicol.* **2022**, *162*, 112907.

[14] Chai, X.; Li, Y. B.; Ma, C. N.; Guo, M. J.; Fan, Z.; Zhao, J.; Cheng, B. W. A voltammetric sensor based on a reduced graphene oxide/β-cyclodextrin/silver nanoparticle/polyoxometalate nanocomposite for detecting uric acid and tyrosine. *Anal. Methods* **2023**, *15*, 2528–2535.

[15] Aslam, M.; Kalyar, M. A.; Raza, Z. A. Synthesis and structural characterization of separate graphene oxide and reduced graphene oxide nanosheets. *Mater. Res. Express* **2016**, *3*, 105036.

[16] dos Santos, J. R. N.; Alves, I. C. B.; Marques, A. L. B.; Marques, E. P. Ni-Ag supported on reduced graphene oxide as efficient electrocatalyst for alcohol oxidation reactions. *Electrocatalysis* **2022**, *13*, 713–730.

[17] Gijare, M. S.; Chaudhari, S. R.; Ekar, S.; Shaikh, S. F.; Al-Enizi, A. M.; Pandit, B.; Garje, A. D. Green synthesis of reduced graphene oxide (rGO) and its applications in non-enzymatic electrochemical glucose sensors. *J. Photochem. Photobiol. A: Chem.* **2024**, *450*, 115434.

[18] Jiang, X. D.; Wang, J. K.; Zhou, B. M. A two-step chemical-hydrothermal reduction method to prepare reduced graphene oxide with high electrical conductivity. *Diamond Relat. Mater.* **2022**, *130*, 109437.

[19] Kumar, N.; Setshedi, K.; Masukume, M.; Ray, S. S. Facile scalable synthesis of graphene oxide and reduced graphene oxide: Comparative investigation of different reduction methods. *Carbon Lett.* **2022**, *32*, 1031–1046.

[20] Verma, V.; Gurnani, L.; Das, A.; Kumari, N.; Dasgupta, T.; Mukhopadhyay, A. Reduced graphene oxides prepared via explosive and non-explosive thermal reduction: Structural evolution, functional properties and reinforcing efficacy. *Carbon* **2023**, *209*, 118007.

[21] Gómez-Mancebo, M. B.; Fernández-Martínez, R.; Ruiz-Perona, A.; Rubio, V.; Bastante, P.; García-Pérez, F.; Borlaf, F.; Sánchez, M.; Hamada, A.; Velasco, A. et al. Comparison of thermal and laser-reduced graphene oxide production for energy storage applications. *Nanomaterials* **2023**, *13*, 1391.

[22] Xian, Z. W.; Liu, R. J.; Li, H.; Zhang, S. S.; Yang, Z. H.; Zheng, W. Q.; Chen, C. H.; Cao, H. B.; Zhang, G. J. Photocatalytic reduction synthesis of ternary Ag nanoparticles/polyoxometalate/graphene nanohybrids and its activity in the electrocatalysis of oxygen reduction. *J. Clust. Sci.* **2016**, *27*, 241–256.

[23] Yang, M. L.; Rong, S.; Wang, X. M.; Ma, H. Y.; Pang, H. J.; Tan, L. C.; Jiang, Y. X.; Gao, K. Q. Preparation and application of keggin polyoxometalate-based 3D coordination polymer materials as supercapacitors and amperometric sensors. *ChemNanoMat* **2021**, *7*, 299–306.

[24] Wang, D.; Liu, L. L.; Jiang, J.; Chen, L. J.; Zhao, J. W. Polyoxometalate-based composite materials in electrochemistry: State-of-the-art progress and future outlook. *Nanoscale* **2020**, *12*, 5705–5718.

[25] Guedes, G.; Wang, S. Q.; Santos, H. A.; Sousa, F. L. Polyoxometalate

composites in cancer therapy and diagnostics. *Eur. J. Inorg. Chem.* **2020**, *2020*, 2121–2132.
[26] Zhang, S. S.; Liu, R. J.; Streb, C.; Zhang, G. J. Design and synthesis of novel polyoxometalate-based binary and ternary nanohybrids for energy conversion and storage. *Polyoxometalates* **2023**, *2*, 9140037–9140037.
[27] Zheng, S. T.; Yang, G. Y. Recent advances in paramagnetic-TM-substituted polyoxometalates (TM = Mn, Fe, Co, Ni, Cu). *Chem. Soc. Rev.* **2012**, *41*, 7623–7646.
[28] Yaqub, A.; Gilani, S. R.; Bilal, S.; Hayat, A.; Asif, A.; Siddique, S. A. Efficient preparation of a nonenzymatic nanoassembly based on cobalt-substituted polyoxometalate and polyethylene imine-capped silver nanoparticles for the electrochemical sensing of carbofuran. *ACS Omega* **2022**, *7*, 149–159.
[29] Li, S.; Ma, H. Y.; O'Halloran, K. P.; Pang, H. J.; Ji, H. R.; Zhou, C. L. Enhancing characteristics of a composite film by combination of vanadium-substituted molybdophosphate and platinum nanoparticles for an electrochemical sensor. *Electrochim. Acta* **2013**, *108*, 717–726.
[30] Zhang, Y. M.; An, C. W.; Zhang, D. F.; Liu, T.; Yan, J. S.; Zhang, J. Photocatalytic activity of vanadium-substituted polyoxometalate doped magnetic carbon nitride towards antibiotics. *Russ. J. Inorg. Chem.* **2021**, *66*, 679–683.
[31] Fernandes, D. M.; Nunes, M.; Carvalho, R. J.; Bacsa, R.; Mbomekalle, I. M.; Serp, P.; De Oliveira, P.; Freire, C. Biomolecules electrochemical sensing properties of a $PMo_{11}V$@N-Doped few layer graphene nanocomposite. *Inorganics* **2015**, *3*, 178–193.
[32] Zhang, L.; Ning, L.; Zhang, Z. F.; Li, S. B.; Yan, H.; Pang, H. J.; Ma, H. Y. Fabrication and electrochemical determination of l-cysteine of a composite film based on V-substituted polyoxometalates and Au@2Ag core-shell nanoparticles. *Sens. Actuators B: Chem.* **2015**, *221*, 28–36.
[33] Chu, M. Y.; Bai, Z. Y.; Zhu, D.; Chen, W. J.; Yang, G. X.; Xin, J. J.; Ma, H. Y.; Pang, H. J.; Tan, L. C.; Wang, X. M. A β-nicotinamide adenine dinucleotide electrochemical sensor based on polyoxometalate built by the combination of electrodeposition and self-assembly. *J. Electroanal. Chem.* **2022**, *907*, 116083.
[34] Yu, S. P.; Zhao, X. H.; Su, G. Y.; Wang, Y.; Wang, Z. M.; Han, K. F.; Zhu, H. Synthesis and electrocatalytic performance of a P-Mo-V Keggin heteropolyacid modified Ag@Pt/MWCNTs catalyst for oxygen reduction in proton exchange membrane fuel cell. *Ionics* **2019**, *25*, 5141–5152.
[35] Dhayagude, A. C.; Newase, S. K.; Joshi, S. S.; Kapadnis, B. P.; Kapoor, S. Preparation of silver nanoparticles in the presence of polyoxometalates. *Mater. Sci. Eng.: C* **2019**, *94*, 437–444.
[36] Wang, Y. Z.; Li, H. L.; Wu, C.; Yang, Y.; Shi, L.; Wu, L. X. Chiral heteropoly blues and controllable switching of achiral polyoxometalate clusters. *Angew. Chem., Int. Ed.* **2013**, *52*, 4577–4581.
[37] Han, H.; Liu, C.; Sha, J. Q.; Wang, Y.; Dong, C. Y.; Li, M. J.; Jiao, T. Y. Ferrocene-reduced graphene oxide-polyoxometalates based ternary nanocomposites as electrochemical detection for acetaminophen. *Talanta* **2021**, *235*, 122751.
[38] Tong, X.; Thangadurai, V. Hybrid gel electrolytes derived from Keggin-type polyoxometalates and imidazolium-based ionic liquid with enhanced electrochemical stability and fast ionic conductivity. *J. Phys. Chem. C* **2015**, *119*, 7621–7630.
[39] Albers, R. F.; Bini, R. A.; Souza, J. B. Jr. *; Machado, D. T.; Varanda, L. C. A general one-pot synthetic strategy to reduced graphene oxide (rGO) and rGO-nanoparticle hybrid materials. Carbon* **2019**, *143*, 73–84.
[40] Zhang, C.; Cui, M.; Ren, J. J.; Xing, Y. F.; Li, N.; Zhao, H. Y.; Liu, P.; Ji, X. P.; Li, M. Facile synthesis of novel spherical covalent organic frameworks integrated with Pt nanoparticles and multiwalled carbon nanotubes as electrochemical probe for tanshinol drug detection. *Chem. Eng. J.* **2020**, *401*, 126025.
[41] Shafiei, H.; Karim Hassaninejad-Darzi, S. Electroanalytical application of Ag@POM@rGO nanocomposite and ionic liquid modified carbon paste electrode for the quantification of ciprofloxacin antibiotic. *J. Electroanal. Chem.* **2023**, *935*, 117321.
[42] Zhu, D.; Bai, Z. Y.; Ma, H. Y.; Tan, L. C.; Pang, H. J.; Wang, X. M. High performance simultaneous detection of β-nicotinamide adenine dinucleotide and $_L$-tryptophan in human serum based on a novel nanocomposite of ferroferric oxide-functionalized polyoxometalates. *Sens. Actuators: B Chem.* **2020**, *309*, 127787.
[43] Xu, Y. L; Niu, X. Y.; Chen, H. L.; Zhao, S. G.; Chen, X. G. Switch-on fluorescence sensor for ascorbic acid detection based on $MoS_2$ quantum dots-$MnO_2$ nanosheets system and its application in fruit samples. *Chin. Chem. Lett*. **2017**, *28*, 338–344.
[44] Hu, J.; Wu, X. F.; Zhang, Q. F.; Gao, M. Y.; Qiu, H. F.; Huang, K. K.; Feng, S. H.; Yang, Y.; Liu, Z. L.; Zhao, B. Preparation of a highly active palladium nanoparticle/polyoxometalate/reduced graphene oxide nanocomposite by a simple photoreduction method and its application to the electrooxidation of ethylene glycol and glycerol. *Electrochem. Commun.* **2017**, *83*, 56–60.
[45] Murtada, K.; Moreno, V. Nanomaterials-based electrochemical sensors for the detection of aroma compounds- towards analytical approach. *J. Electroanal. Chem.* **2020**, *861*, 113988.
[46] Kumari, R.; Kumar, H.; Yadav, A.; Sharma, R.; Kumari, A.; Kumar, A. Metal nanocomposites-based electrochemical sensor for the detection of vanillin (food additives): Experimental and theoretical approach. *Food Biosci.* **2023**, *52*, 102464.
[47] Haghighi, B.; Rahmati-Panah, A.; Shleev, S.; Gorton, L. Carbon ceramic electrodes modified with laccase from *Trametes hirsuta*: Fabrication, characterization and their use for phenolic compounds detection. *Electroanalysis* **2007**, *19*, 907–917.
[48] Silva, T. R.; Brondani, D.; Zapp, E.; Vieira, I. C. Electrochemical sensor based on gold nanoparticles stabilized in poly (allylamine hydrochloride) for determination of vanillin. *Electroanalysis* **2015**, *27*, 465–472.
[49] Lahouidak, S.; Salghi, R.; Zougagh, M.; Ríos, A. Capillary electrophoresis method for the discrimination between natural and artificial vanilla flavor for controlling food frauds. *Electrophoresis* **2018**, *39*, 1628–1633.
[50] Sordoń, W.; Jakubowska, M. Electrochemical evaluation and voltammetric determination of some phenolic acids on the boron-doped diamond electrode. *Diamond Relat. Mater.* **2023**, *138*, 110236.

**Shixu Chen** is a Master's student at the School of Sciences, Hebei University of Science and Technology. His research interests are electrochemical sensing based on polyoxometalates.

**Cong Zhang** is an associate professor at the School of Sciences, Hebei University of Science and Technology. His research is focused on the chemical and biological sensing based on polyoxometalates-based functional materials.